A Novel Σ–Δ Pulsed Digital Oscillator (PDO) for MEMS

Manuel Domínguez, *Member, IEEE*, Joan Pons-Nin, *Member, IEEE*, Jordi Ricart, Agustín Bermejo, and Eduardo Figueras Costa

***Abstract*—A novel digital oscillator topology for microelectromechanical systems (MEMS) based on bandpass sigma–delta modulation is presented. Short pulses of force of the same amplitude maintain the oscillation and the associated bit-stream output serves to know the oscillation frequency which, for low mechanical losses, is very close to the natural frequency of the MEMS resonator. Position-sensing requirements are extremely simplified because, at each sampling time, it is only necessary to know whether the resonator position is above or below the steady-state position. Continuous-time simulations are presented showing the behavior of the oscillator for different sampling frequencies and mechanical damping losses. Experimental results from an oscillator using a MEMS resonator with thermoelectric actuation and piezoresitive position sensing are presented. It is concluded that the quality of the oscillator response depends on the resonator damping losses and on the sampling frequency. The experimental results agree with the analytical and simulation results.**

***Index Terms*—Microelectromechanical systems (MEMS), oscillator, sigma–delta (Σ–Δ).**

I. Introduction

THE USE OF mechanical resonators is widely extended in many applications, such as the measure of strain and mass change (gravimetric sensors) and as a part of inertial sensors, such as gyroscopes [1]–[3] or accelerometers [4], [5]. Mechanical resonators may be excited by an external oscillator or may be a part of the oscillator itself (self-sustained oscillation).

Microelectromechanical systems (MEMS) technologies have provided the grounds for new resonator designs, reducing their size, and providing high-quality factors and output frequencies. However, nonlinearities in actuation or position sensing of MEMS resonators are common problems in MEMS drive, specifically in the design of large-signal oscillators. Moreover, large-signal oscillators with simple topologies have been proposed [6], but they exhibit chaotic behavior and do not produce sinusoidal signals at the output.

Manuscript received November 18, 2003; revised August 2, 2004. This work was supported by the CICYT-TIC-2001-2163 project. The associate editor coordinating the review of this paper and approving it for publication was Prof. Fabien Josse.

M. Domínguez, J. Pons-Nin, J. Ricart, and A. Bermejo are with the Semiconductor Devices Group, Department of Electronic Engineering, Universitat Politécnica de Catalunya, 08034 Barcelona, Spain (e-mail: mpumar@eel.upc.es; jpons@eel.upc.es; ricart@eel.upc.es; agus@metropoli2000.net)

E. Figueras Costa is with the Instituto de Microelectrónica de Barcelona (IMB-CNM, CSIC), 08193 Bellaterra, Barcelona, Spain (e-mail: eduard.figueras@cnm.es).

Digital Object Identifier 10.1109/JSEN.2005.855601

MEMS devices are actuated through thermoelectric or electrostatic forces, among others. One of the main characteristics of these actuation principles is the nonlinearity they exhibit. In the parallel-plate capacitor approximation of a MEMS device with electrostatic actuation, the electrical force applied to the moveable plate is proportional to the square of the electrical charge stored in the capacitor

$$F(t) = \frac{Q^2(t)}{2\varepsilon A} \tag{1}$$

where $\mathrm{Q(t)}$ is the stored charge, A is the area of the capacitor, and ε is the dielectric constant. In the case of thermoelectric actuation, the mechanical force is proportional to the power dissipated in a nearby resistor. This way, the force is proportional to the square of the applied voltage or current. These actuation principles constitute a set of actuation variables, which are clearly nonlinear but at the same time, are independent of the position of the MEMS resonator. This is not the case, for example, of electrostatic actuation with voltage drive, where the applied force is

$$F(t) = \frac{A\varepsilon V^2(t)}{2(g_0 - x(t))^2} \tag{2}$$

where $V(t)$ is the applied voltage, $\mathrm{g_0}$ is the capacitor gap, and $x(t)$ is the plate position. The mechanical force clearly depends on the position of the MEMS resonator.

In the first two cases, in the absence of bias, the position-independent mechanical force created has twice the frequency of the applied ac drive [7], making then necessary a frequency division in the feedback loop in any conventional oscillator topology. In the topology proposed here, this is solved by using a binary feedback in the oscillator loop, i.e., pulses of force that can only take two values $\{+F, -F\}$. This, in turn, provides an overall nonperfect feedback signal, which is filtered by the resonator itself, producing in the end a good spectrum for resonators with low damping losses (and, thus, high-Q factors). The topology of the oscillator is shown in Fig. 1. It uses short pulses of force and the oscillation frequency can be extracted from the bit stream at the output of the oscillator. The position-sensing requirements are also extremely simplified, because it is only necessary to know, at each sampling time, whether the MEMS resonator is above or below its steady-state position. This way, both nonlinearities in actuation and position sensing can be easily overcome.

This work extends the results in [8] by experimentally demonstrating the oscillation of a circuit using MEMS cantilever with thermoelectric actuation. As will be shown, the obtained results

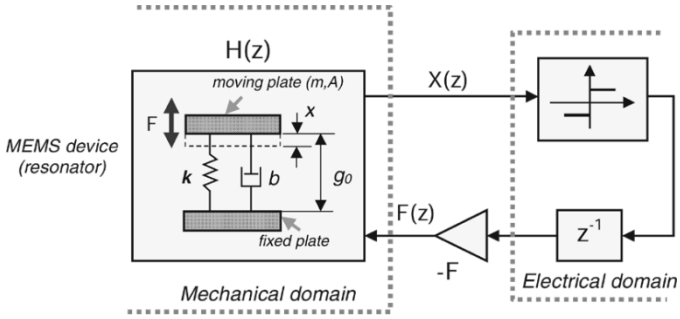

Fig. 1. Oscillator topology and 1-D mechanical model for the MEMS device.

closely follow the behavior predicted by the linear analysis and the continuous-time simulations. Extensive experimental measurements have been carried out, for different sampling frequencies and for different damping conditions. The output spectrum, as expected, improves for lower damping losses and the oscillation frequency can be extracted from the output bit stream.

The oscillator topology is presented and analyzed in Section I by using linear systems theory and standard sigma–delta (Σ–Δ) approximations, such as a uniform quantization noise. In Section II, results from extensive simulations for a realistic reference case are shown and some key ideas about the oscillator performance are extracted. Finally, experimental results obtained from a prototype are presented and checked in Section III. In Sections II and III, the oscillation frequency of the resonator is evaluated through the calculation of the FFT of the bitstream or of the position of the resonator.

II. Oscillator Linear Analysis

The topology of the oscillator proposed in this work is shown in Fig. 1. A two parallel-plate MEMS actuator is used as a resonator. The feedback loop is similar that of a bandpass Σ–Δ modulator due to the presence of a resonator, although, of course, no input signal is present.

The key characteristics of the structure are as follows.

- It is a pulsed system. Short force pulses of values $\pm$F are used to ensure oscillation. Thus, nonlinearity in actuation is avoided as only two constant values of force are used.
- Position sensing is required only at fixed intervals (sampling frequency), and it is only necessary to know whether the resonator is above or below the steady-state position $(\mathrm{x} = 0)$.
- The oscillation frequency can be determined by calculating the spectrum of the bit stream at the output of the binary quantizer.

Let us now analyze the behavior of the structure proposed in Fig. 1. The dynamics of the mechanical resonator, actuated through an electrostatic field, can be approximated by a one-dimensional (1-D) second-order spring-mass system characterized by the following linear equation [9]:

$$m\frac{d^2x(t)}{dt^2} + b\frac{dx(t)}{dt} + kx(t) = F(t) \tag{3}$$

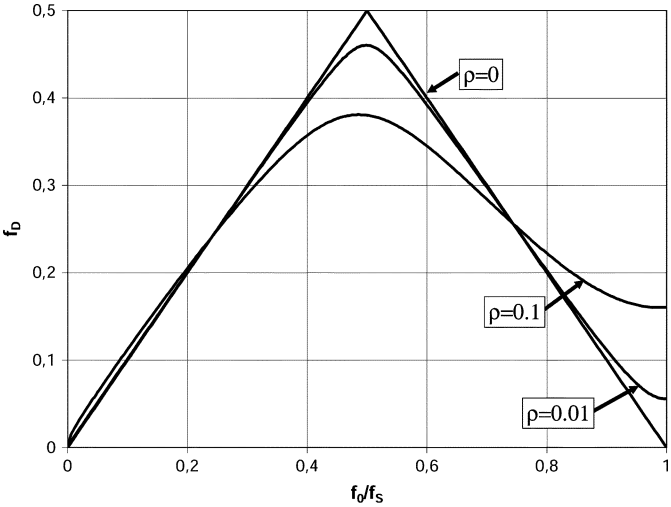

Fig. 2. Normalized digital oscillation frequency as a function of the sampling ratio for different values of the damping losses.

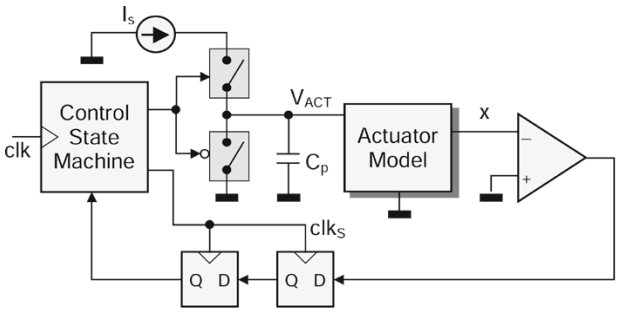

Fig. 3. Saber simulations schematic.

TABLE I
Parameter Values of the MEMS Device Used in the Simulations

m	*3.23e-9 Kg*
k	*0.521 N/m*
b	*6.76e-7 Ns/m*
g0	*3 μm*
A	*250x250 μm²*

where x and m are, respectively, the position and the mass of the moveable plate, b is the damping factor, k is the spring factor, and F is the external applied force. The Laplace transform of the mechanical impulse response of the resonator is

$$H(s) = X(s)/F(s) = \frac{1}{m(s^2 + 2\rho\omega_0 s + \omega_0^2)} \tag{4}$$

where ρ and ω_0 are the dimensionless damping factor and the resonant frequency of the resonator

$$\rho = \frac{b}{\sqrt{km}} \quad \omega_0 = \sqrt{\frac{k}{m}}. \tag{5}$$

As any sampled structure, the oscillator is a discrete-time system. In order to analyze the feedback loop, the z transform

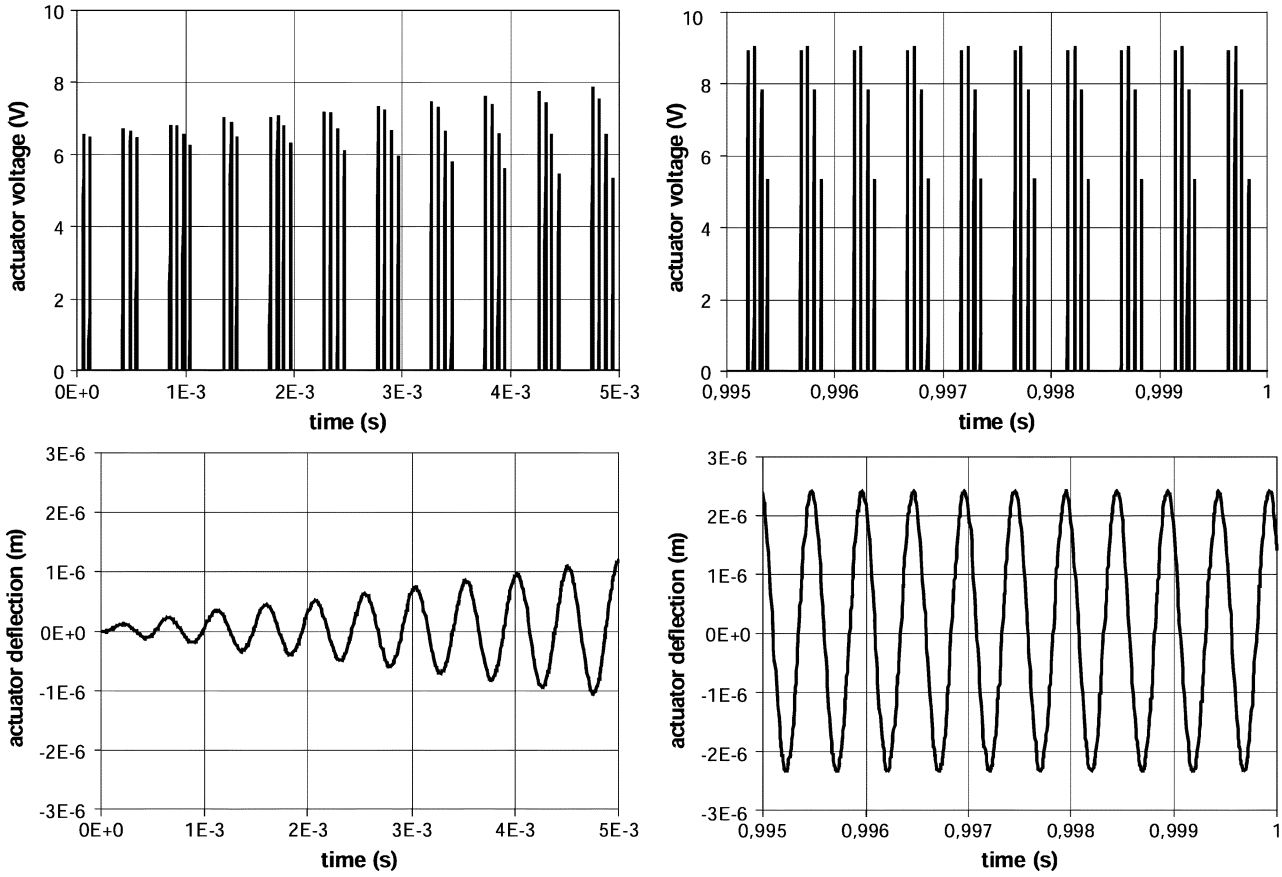

Fig. 4. Transient and stationary waveforms of the actuator voltage and position for $f_S = 8f_0$ and $C_P = 0.1$ pF.

of $H(s)$ for a given sampling frequency ($f_S = 1/T_S$) is found to be

$$H(z) = \frac{K_n z^{-1}}{1 - \alpha z^{-1} + \beta z^{-2}}. \tag{6}$$

Parameters K_n, α, and β can be obtained straightforwardly from the sampled impulse response of the mechanical resonator [10]

$$\begin{aligned} K_n &= \frac{e^{-\rho\omega_0 T_S}\sin(\omega_0 T_S\sqrt{1-\rho^2})}{m\omega_0\sqrt{1-\rho^2}} \\ \alpha &= 2e^{-\rho\omega_0 T_S}\cos(\omega_0 T_S\sqrt{1-\rho^2}) \\ \beta &= e^{-2\rho\omega_0 T_S}. \end{aligned} \tag{7}$$

In the preceding analysis, we have used the impulse invariant method to find the sampled impulse response $H(z)$ of the resonator. Other methods usually found in the literature to obtain a digital filter with a similar frequency response to that of a given analog filter (as in the case of the bilinear transform method) can not be used. Here, the real sampled response of the oscillator is needed, even when the clock frequency of the oscillator is below the Nyquist frequency, and, therefore, aliasing occurs in the bit stream.

Let us now consider that the binary quantizer introduces a white uniform noise. This is a standard approximation in the analysis of Σ–Δ modulators. Then, the characteristic equation of the oscillator is

$$1 - \alpha z^{-1} + (\beta + FK_n)z^{-2}. \tag{8}$$

By adjusting the value of F to $(1-\beta)/K_n$, it is possible to force an oscillation in the circuit. However, in our case, it is clear that this is not a necessary condition. The bit stream at the output of the binary quantizer remains constant as a function of the force delta area (F), which only acts as a scaling factor of the position waveform of the MEMS device, and, thus, does not change the output of the quantizer. It will be shown later in Section II, however, that the sign of F must be the sign of $(1-\beta)/K_n$ in order to have a sustained oscillation.

The resulting oscillation frequency is $f_D f_S$, where f_D, called the normalized digital oscillation frequency, is given by the following expression [11]:

$$f_D = \frac{1}{2\pi}\cos^{-1}\left(e^{-\rho 2\pi f_0/f_S}\cos\left(2\pi\frac{f_0}{f_S}\sqrt{1-\rho^2}\right)\right). \tag{9}$$

Equation (9) implies that the oscillation frequency is a function of the sampling frequency, the mechanical resonator, and its damping losses. It is interesting to see that, for a system with no damping losses ($\rho \cong 0$) and $0 < f_0/f_S < 1/2$, the oscillation frequency is equal to the natural frequency of the mechanical

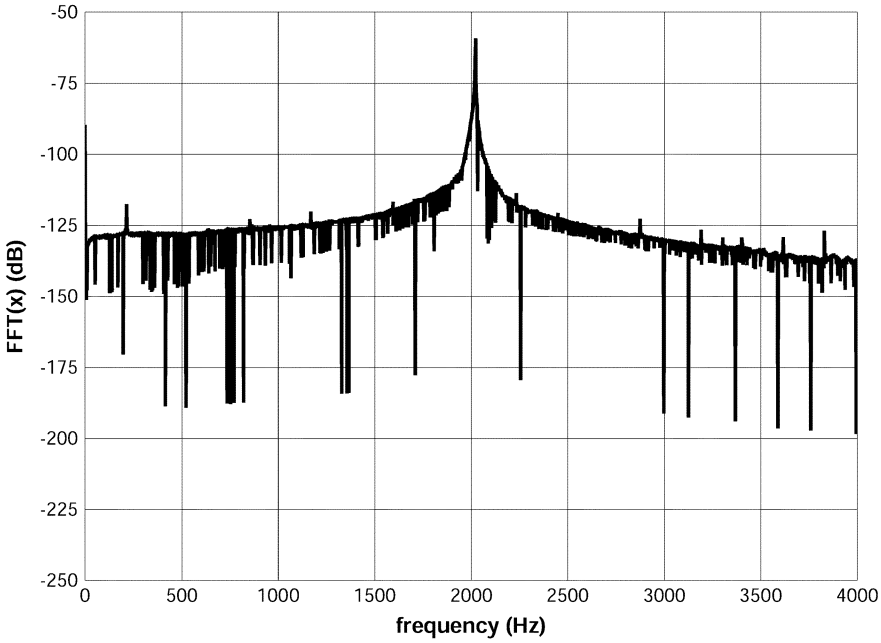

Fig. 5. Actuator position spectrum for $f_S = 8f_0$ and $C_P = 0.1$ pF.

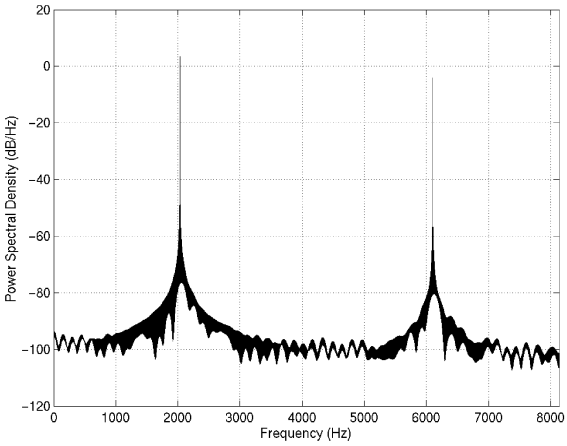

Fig. 6. Power spectral density of the bit-stream output for $f_S = 8f_0$ (bits $= 1$ or -1), obtained with 128-K samples.

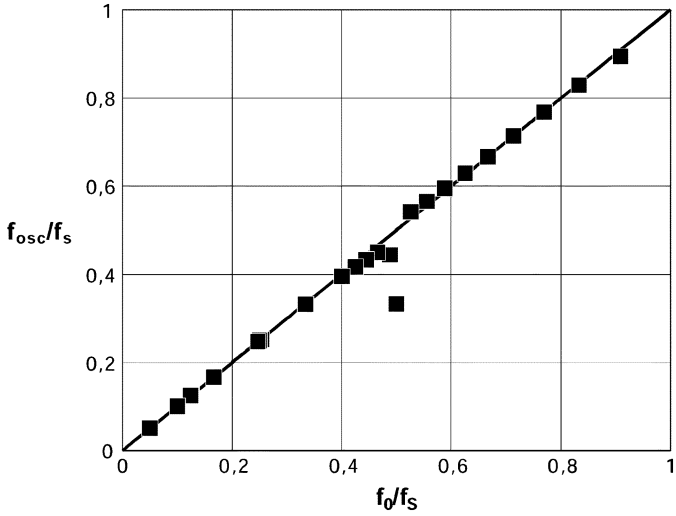

Fig. 7. Normalized digital oscillation frequency as a function of f_0/f_S for $C_P = 0$.

resonator ($f_D f_S = f_0$). This is observed in Fig. 2, where plots of f_D as a function of the sampling ratio f_0/f_S for three different damping values are shown. It is also observed that a loss of linearity between f_D and f_0/f_S appears and becomes more evident for increasing values of the damping loss factor.

For sampling frequencies in the range $1/2 \leq f_0/f_S \leq 1$, aliasing occurs, and, although the structure is oscillating at frequencies close to f_0, the values of the normalized digital oscillation frequency provided by linear theory remain in the range $0 \leq f_D \leq 1/2$.

III. Simulation Results

Extensive continuous-time simulations have been carried out using Synopsys Saber. In this case, a MEMS device with electrostatic actuation has been considered. The "ideal" oscillator structure shown in Fig. 1 and discussed in the previous section considers that it is possible to give at each sampling period a force delta of $+F$ or $-F$ area, so overcoming the nonlinearities in actuation. Simulations to check the behavior and the performance of the oscillator and their coherence with linear theory are now needed. Then, a more realistic point of view is applied and some new factors and effects are now considered.

- Force actuation cannot be based on pure deltas, but on short pulses of charge fed into the resonator capacitance. Then a charge drive circuit is needed.
- The electrostatic force is usually attractive, although recently repulsive electrostatic forces with nonvolatile charge have been used [12]. Then, the comparator output is "1" or "0"and the resonator drive consists on supplying a pulsed charge (i.e., current pulse) or setting to zero the charge stored in the actuator capacitance (i.e., a short circuit).

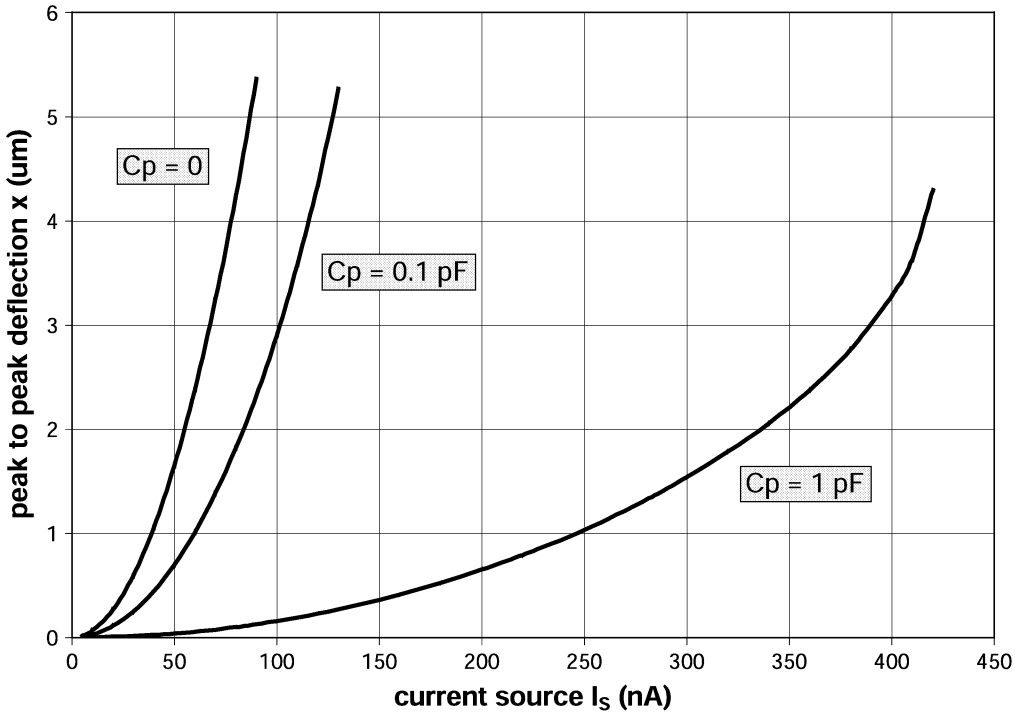

Fig. 8. Oscillation amplitude as a function of the current source level for $f_S = 4 f_0$.

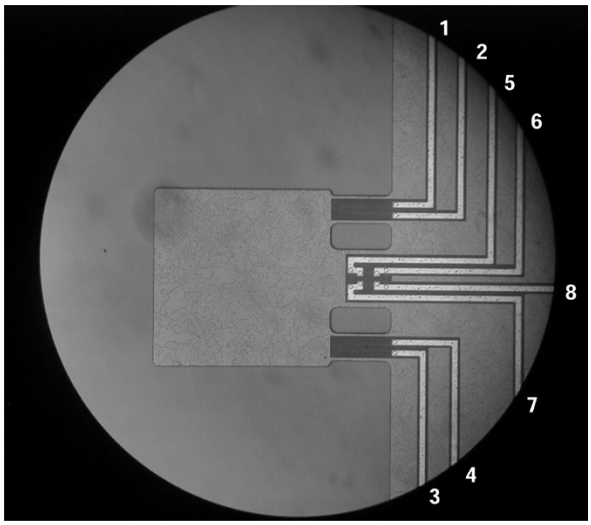

Fig. 9. Top view of the MEMS actuator used in the measurements.

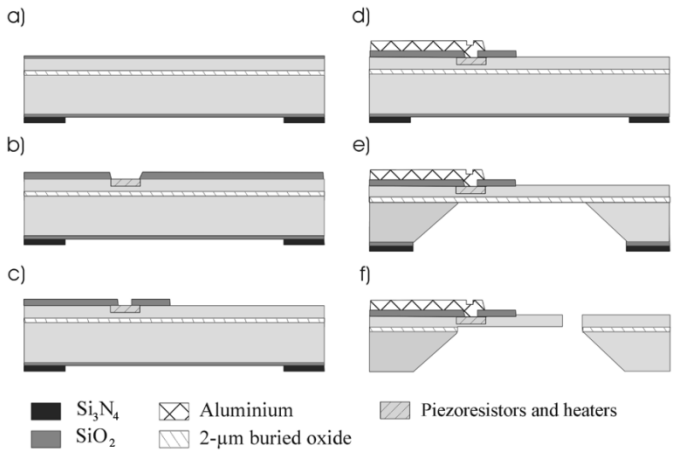

Fig. 10. Fabrication steps of the MEMS resonator.

- In any charge drive circuit, effects such as a parasitic capacitance in parallel with the resonator capacitance can be relevant and must be taken into account [9].

To this purpose, detailed models of the electronic and mechanical parts of the oscillator have been considered and extensive mixed-domain Saber simulations have been carried out. A model based on (1) and (3) and written in the analog MAST language has been used to describe the MEMS actuator as a behavioral module. The complete simulation structure of the oscillator is shown in Fig. 3. Charge is provided by a pulsed current source. Delays, pulse lengths, and sample frequencies are provided by a synchronous finite-state machine. Constant current pulse lengths of 5 μs have been used in the simulations. A parasitic capacitance C_P has also been included.

A real MEMS actuator data set taken from the literature [13] has been used as a reference case in the simulations, with a damping coefficient $b = 6.76e$-7 Ns/m [14]. Values of the mechanical parameters of this device are listed in Table I. The resonant frequency and the dimensionless damping factor values are $f_0 = 2021$ Hz and $\rho = 8.24e$-3.

Fig. 4 is an example of the simulation results obtained for $f_S = 8 f_0$ and $C_P = 0.1$ pF. It shows a snapshot of the transient and stationary regimes both for the input voltage and the position of the actuator. The short-pulse shape of the input voltage is a consequence of the constant current pulses (or fixed amounts of charge) fed into the actuator capacitance. The maximum value of each voltage pulse is not the same because the actuator capacitance depends on its position [9]. On the other hand, the position waveform has an almost perfect sinusoidal shape and exhibits a large amplitude of 2.4 μm from

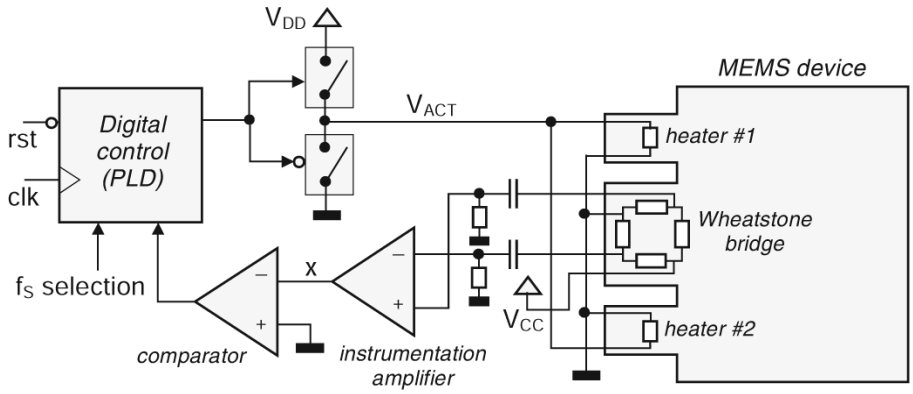

Fig. 11. Experimental setup.

a $g_0 = 3\ \mu$m gap. Moreover, as it is expected from the charge drive mode used in this oscillator [9], no problems arise when the actuator position exceeds the pull-in value ($g_0/3 = 1\ \mu$m). A small position offset of 42 nm has also been observed. This offset exists because the actuation pulses are always positive or zero, so a certain dc level at the output of the actuator must be expected. Finally, let us note that in this example the binary output in the stationary regime becomes a periodical sequence composed by four "1s followed by four 0s."

Fig. 5 shows the position spectrum for the same situation as in Fig. 4. The maximum peak is located at $f_0 = 2021$ Hz. As expected from previous discussions, a tone at zero frequency is observed, meaning that a constant offset is added to the position. Fig. 6 shows the spectrum of the bit-stream output, obtained through a Matlab simulation of the oscillator (considered as a discrete-time system), for the same situation as in Fig. 5, but $C_P = 0$. As can be observed, both spectrums are very similar near the resonance frequency of the MEMS device.

Fig. 7 shows the normalized oscillation frequency $f_{\rm osc}/f_S$ as a function of the sampling ratio f_0/f_S for the reference device and $Cp = 0$. In the simulations of Fig. 7, the oscillation amplitude is kept constant by adjusting the value of the current source I_S. As can be seen, the results closely follow the tendency predicted by the linear theory. It is also shown that sampling ratio values beyond the Nyquist frequency ($f_0/f_S > 1/2$) still exhibit an oscillation frequency close to the resonance frequency of the MEMS device. The sign of the feedback signal fed into the resonator, however, must be changed in order to have a sustained simulation.

Extensive Saber simulations with nonnegligible values of the parasitic capacitance C_P have also been carried out. The main conclusion extracted from the results is that C_P has a small influence on the oscillation frequency. This influence is observed only for C_P values much larger than the electrical capacitance of the actuator. It is interesting to note that when $Cp > 0$, there is a certain charge sharing between the parasitic and MEMS capacitances. The first capacitor does not depend on the position of the MEMS device, whereas the second does. Thus, the resulting electrostatic force in charge drive is

$$F(t) = \frac{A\varepsilon}{2}\frac{Q^2(t)}{(C_P(g_0 - x(t)) + A\varepsilon)^2} \qquad (10)$$

which is position dependent. Then, the fact that the continuous time simulations shows that oscillator still works for $C_P > 0$, unless the parasitic capacitance is much larger than the MEMS capacitance, has an added value, because it shows that the oscillator can work under some conditions when a position-dependent force is used.

On the other hand, for a given current source level I_S, both the oscillation amplitude and offset have a strong dependence on the value of C_P. The magnitude of the force pulses does not prevent the circuit from oscillating, as expected. Fig. 8 shows the oscillation amplitude as a function of I_S for three different values of C_P. As can be observed, the main effect of the parasitic capacitance is a decrease of the oscillation amplitude, because at each current pulse the charge is shared between both the parasitic and the electrical capacitance of the actuator. Results also show that the oscillation offset has exactly the same behavior than the amplitude, but with smaller values.

Finally, it is interesting to note that the pulsed digital oscillator (PDO) has not the characteristic shaping of the quantization noise that is usual in Σ–Δ modulators. Although the topology of the PDO is very similar to a bandpass Σ–Δ modulator, it is not exactly the same circuit. This way the usual properties of Σ–Δ modulation should not be assumed. This has been confirmed in the simulations shown here and also in the experimental results of Section III. When a resonator with low damping losses is used, the bit stream at the output of the oscillator is that of the sign of a sampled sinusoid, thus, differing from the usual bit stream of a bandpass Σ–Δ modulator.

These conclusions can be applied to other position-independent actuation forces (as in the case of the thermoelectric actuation) and other resonator structures.

IV. Experimental Results

A prototype of the oscillator for a MEMS cantilever with thermoelectric actuation and piezoresistive sensing has been fabricated. Fig. 9 shows a microphotograph of the MEMS resonator used in the experimental measurements. It has a silicon cantilever with thermoelectric actuation through two heaters (electrodes 1 to 4). The cantilever dimensions are 300 μm long, 300 μm wide, and 5 μm thick. Position feedback is obtained through a piezoresistive Wheatstone bridge (electrodes 5 to 8).

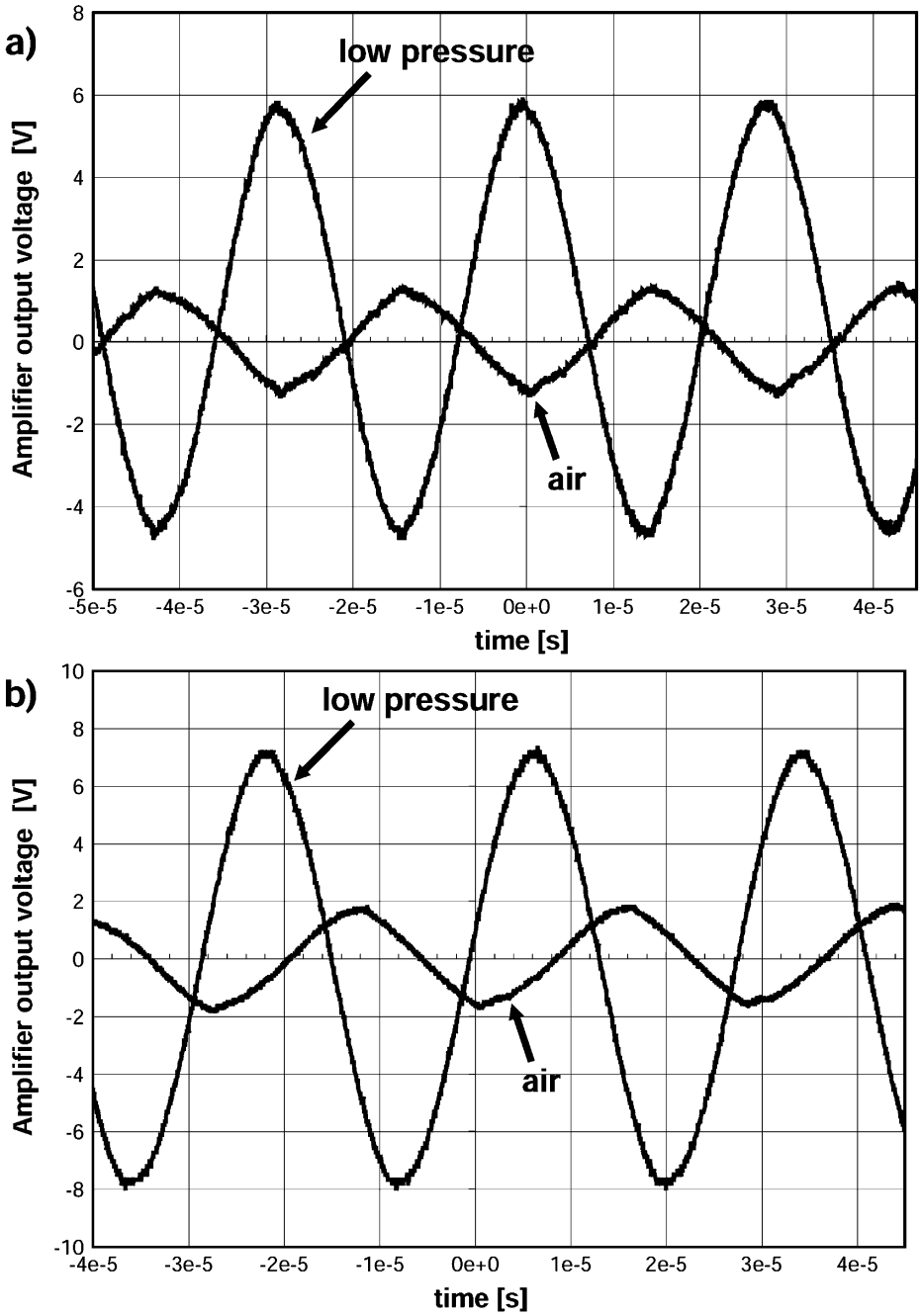

Fig. 12. Measured waveforms of the actuator position for (a) $f_S = 8f_0$ and (b) $f_S = 10f_0$.

The fabrication process starts growing a thin thermal oxide and depositing a LPCVD silicon nitride layer on a SOI N-type substrate. The nitride layer is removed from the front side of the wafer and is patterned at the backside [first mask, Fig. 10(a)]. A boron implantation (second mask) creates the heaters and the piezoresistive bridge [Fig. 10(b)]. A new oxide is grown and then patterned [third mask, Fig. 10(c)]. After an aluminum deposition, the fourth mask defines the metal lines [Fig. 10(d)]. With the nitride layer acting as a mask, the silicon substrate is etched from the backside using a KOH etch that stops at the SOI buried oxide [Fig. 10(e)], which is afterwards removed. Finally, the SOI layer is patterned with the last mask to define the structures [Fig. 10(f)].

The mechanical movement of the resonator has been measured with a vibrometer and a natural resonance frequency near $f_0 = 35.8$ kHz has been obtained. Fig. 11 shows the topology of the oscillator used in the measurements. The force pulses are obtained from short voltage pulses provided by open-drain transistors. The control finite-state machine has been implemented on a low density PLD.

In order to experimentally check the dependence of the oscillator behavior on the resonator damping losses, we have made measurements both at ambient pressure and at low pressure (0.05 mbar). In ambient pressure, the damping losses are much higher than in low pressure, so differences in the oscillation amplitude and in the quality of the output waveforms are

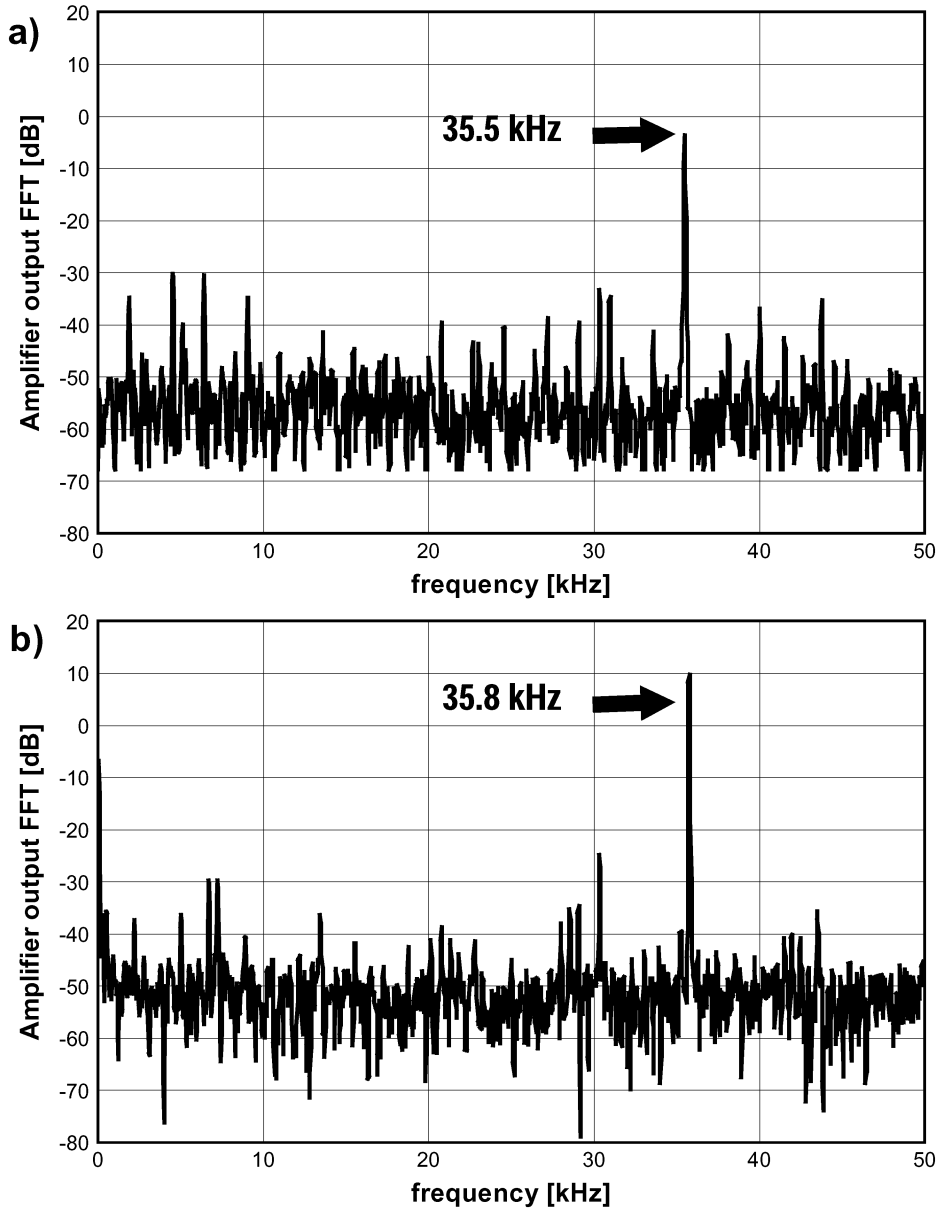

Fig. 13. Spectrums of the actuator position for (a) $f_S = 8f_0$ measured on air (b) and low pressure.

easily observed. As an example, Fig. 12 shows the position waveforms, measured at the amplifier output, for both pressure cases and two sampling ratios, $f_S = 8f_0$ and $f_S = 10f_0$. Let us note that low pressure (or low damping) measurements always exhibit good sinusoidal waveforms.

Fig. 13 shows the position spectrums obtained for both pressure cases and a sampling ratio $f_S = 8f_0$. We can see that, as expected, the quality of the spectrum is better in the case of low damping losses, and the maximum is located at the mechanical resonant frequency f_0. Besides, a small shift of 300 Hz in the exact location of the maximum can be also observed; that is, for larger damping losses, the oscillation frequency becomes lower.

Finally, Fig. 14 shows the spectrum of the bit stream at the output of the binary quantizer (1-Hz resolution) and the spectrum of the MEMS position (100-Hz resolution). According to previous discussion, the real oscillation frequency can be extracted from the spectrum of the binary quantizer output. The difference of 39 Hz can be explained by the lower frequency resolution of the MEMS position spectrum.

V. Conclusion

A novel digital oscillator for MEMS based on bandpass Σ–Δ modulation has been presented. It has a simple topology and the binary feedback signal is made of force pulses directly fed into a MEMS resonator. The associated bit stream can be used to determine the oscillation frequency without continuously tracking the position of the resonator. Moreover, the position-sensing requirements are extremely simple because the only necessary information is whether the resonator is above or below its rest position at each sampling time.

Extensive mechanical-electrical simulations have been performed. They show that, in good agreement with theoretical results, the oscillation frequency follows the natural frequency

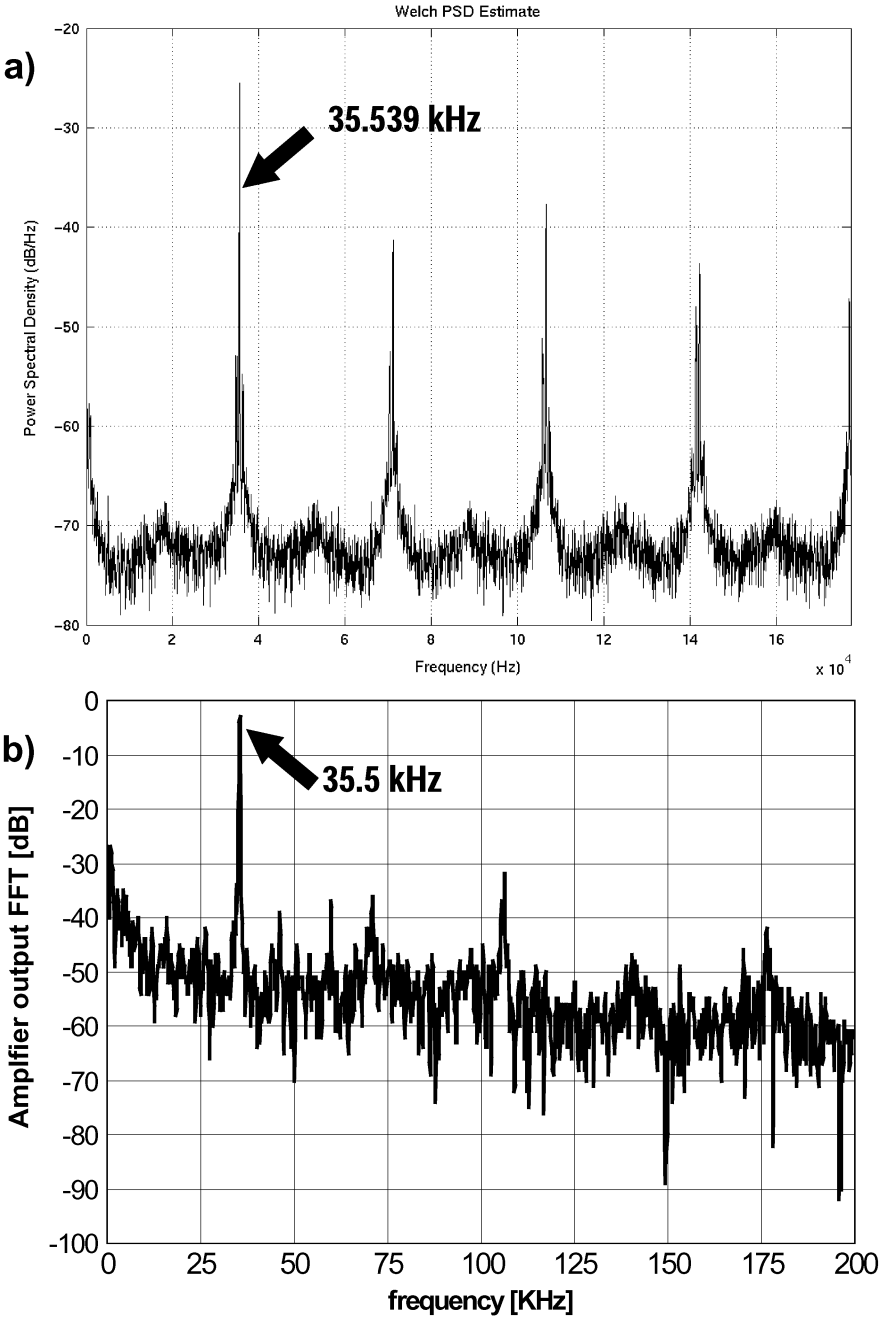

Fig. 14. Spectrums obtained from (a) the bit stream with 64-K samples and from (b) the amplifier output for air and $f_S = 10f_0$.

of the resonator for low damping losses. It is concluded that the quality of the oscillator response depends on the resonator damping losses and on the sampling frequency. In particular, for severe damping losses, higher sampling frequencies must be used.

Finally, experimental results of the PDO using a MEMS resonator with thermoelectric actuation and piezoresistive position sensing have presented. These measurements have been done at ambient pressure (high damping losses) and low pressure (low damping losses). The obtained results agree with the set of conclusions obtained from theory and simulations.

ACKNOWLEDGMENT

The authors wish to thank Prof. L. Castañer and Prof. R. Alcubilla for their fruitful discussions.

REFERENCES

[1] A. J. Harris, J. S. Burdess, J. Cruickshank, D. Wood, and G. Cooper, "A silicon membrane gyroscope with electrostatic actuation," in *Proc. IEE Colloq. Silicon Fabricated Inertial Instruments*, London, U.K., 1996, pp. 5/1–5/7.

[2] S. Lee, S. Park, J. Kim, S. Lee, and D.-I. Cho, "Surface/bulk micromachined single-crystalline-silicon micro-gyroscope," *J. Microelectromech. Syst.*, vol. 9, no. 4, pp. 557–567, 2000.

[3] L. Hao, Z. Xu, H. Lakdawala, L. R. Carley, and G. K. Fedder, "A copper CMOS-MEMS Z-axis gyroscope," in *Proc. Micro Electro Mechanical Systems*, Las Vegas, NV, 2002, pp. 631–634.

[4] S. Sung, J. G. Lee, T. Kang, and J. W. Song, "Development of a tunable resonant accelerometer with self-sustained oscillation loop," in *Proc. NAECON*, Dayton, OH, 2000, pp. 354–361.

[5] B.-L. Lee, C.-H. Oh, S. Lee, Y.-S. Oh, and K.-J. Chun, "A vacuum packaged differential resonant accelerometer using gap sensitive electrostatic stiffness changing effect," in *Proc. MEMS*, Miyazaki, Japan, Jan. 2000, pp. 352–357.

[6] J. Bienstman, R. Puers, and J. Vandewalle, "Periodic and chaotic behavior of the autonomous impact resonator," in *Proc. MEMS*, 1998, pp. 562–567.
[7] J. Bienstman, H. A. C. Tilmans, M. Steyaert, and R. Puers, "An oscillator circuit for electrostatically driven silicon-based one-port resonators," in *Proc. Eurosensors IX Transducers*, 1995, pp. 146–149.
[8] M. Domínguez, J. Pons, J. Ricart, and A. Bermejo, "A sigma-delta digital oscillator for MEMS," in *Proc. IEEE Sensors*, vol. 2, Toronto, ON, Canada, 2003, pp. 834–838.
[9] L. Castañer, J. Pons, R. Nadal-Guardia, and A. Rodríguez, "Analysis of the extended operation range of electrostatic actuators by current-pulse drive," *Sens. Actuators A*, vol. 90, pp. 181–190, 2001.
[10] G. K. Fedder and R. T. Howe, "Multimode digital control of a suspended polysilicon microstructure," *J. Microelectromech. Syst.*, vol. 5, no. 4, pp. 283–297, 1996.
[11] A. V. Oppenheim and R. W. Schafer, *Discrete-Time Signal Processing*. Upper Saddle River, NJ: Prentice-Hall, 1999.
[12] L. Zengtao, K. Myongseob, N. Shen, and E. C. Kan, "Novel electrostatic repulsion forces in MEMS applications by nonvolatile charge injection," in *Proc. MEMS*, 2002, pp. 598–601.
[13] S. P. Pacheco, L. P. B. Katehi, and C. T. Nguyen, "Design of low actuation voltage RF MEMS switch," in *Proc. IEEE MTT-S Int. Microwave Symp. Dig.*, vol. 1, 2000, pp. 165–168.
[14] S. Pacheco, C. T. Nguyen, and L. P. B. Katehi, "Micromechanical electrostatic K-band switches," in *Proc. IEEE MTT-S Int. Microwave Symp. Dig.*, vol. 3, 1998, pp. 1569–1572.

Manuel Domínguez (M'98) received the M.Sc. and Ph.D. degrees from the Department of Electronic Engineering, Universitat Politécnica de Catalunya (UPC), Barcelona, Spain, in 1994 and 1997, respectively.

He has been with the UPC since 1994, where he is now Associate Professor. His research areas include the design and development of MEMS sensors and actuators, cMUTs, sigma–delta modulation applied to MEMS, and the analysis of nonlinear circuits for MEMS. He has participated in several projects, including the design of a flowmeter for home appliances, a light-source position microsensor for the accurate positioning of heliostats in solar concentration plants, and the design of MEMS actuation circuits with voltage pumps. He has coauthored more than 15 scientific papers in international journals and conferences.

Joan Pons-Nin (M'98) received the Ingeniero Superior de Telecomunicación and the Ph.D. degree from the Universitat Politécnica de Catalunya (UPC), Barcelona, Spain, in 1989 and 1995, respectively.

He is an Associate Professor with the Department of Electronic Engineering, UPC. He is currently working on energy and control optimization of electrostatic actuators. Before focusing on electrostatic actuators, he worked on emitter characterization and optimization for advanced bipolar devices and polysilicon contacted silicon solar cells. Semiconductor devices simulation and digital control circuitry are also research topics which interest him.

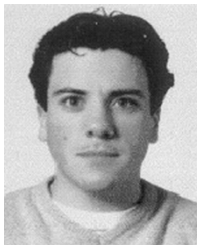

Jordi Ricart was born in Madrid, Spain, in 1975. He received the M.Sc. degree in ingeniería electrónica from the Universitat Politécnica de Catalunya (UPC), Barcelona, Spain, in 2004, where he is currently pursuing the Ph.D. degree.

He joined the Semiconductor Devices Group, Electronic Engineering Department, UPC, as both a Research Assistant and a Ph.D. student. He has worked in photovoltaic processes and thermal flow meter fabrication. His research interests also include the design of specific circuits for MEMS, such as oscillators.

Agustín Bermejo was born in San Sebastian, Spain, in 1979. He received the M.Sc. degree in ingeniería electrónica from the Universitat Politȓcnica de Catalunya (UPC), Barcelona, Spain, in 2004.

He joined the Semiconductor Devices Group, Electronic Engineering Department, UPC, as a Research Assistant. He has worked in MEMS actuation with charge umps. His research interests also include the design of specific circuits for MEMS, such as oscillators.

Eduardo Figueras Costa was born on March 14, 1959, in Barcelona, Spain. He received the degree in physics from the Universitat Autonoma de Barcelona in 1983 and ant the Ph.D. degree in physics from the Universitat Autonoma de Barcelona in 1988.

From 1983 to 1984, he was an Assistant Professor with the Electronics Department, Universitat Autonoma de Barcelona. From 1985 to 1988, at the Microelectronic Laboratory of the Université Catholique de Louvain, Louvain, Belgium, he worked on improvements of isolation oxide in CMOS. In 1989, he obtained a post at the Microelectronic National Centre (CNM), Instituto de Microelectrónica de Barcelona, as a Tenured Scientist (Científico Titular). Until 1998, as a Clean Room Manager at CNM, he supervised all technological processes developed at CNM and was responsible for the standardization of all new fabrication processes, and he is currently with the Microsystems and Silicon Technologies Department, dealing mainly with gas sensors and surface and bulk micromachining. Since 1999, his main activity has been focused on microsystem fabrication processes. The projects he is presently working on are aimed at the development of micromachined resonant devices to be used as gas sensors.